Optical and Quantum Electronics (2023) 55:1143
https://doi.org/10.1007/s11082-023-05296-5

Zinc selenide based dual-channel SPR optical biosensor for HIV genome DNA hybridization detection

Mohamed El-assar[1] · Taha E. Taha[1] · Fathi E. Abd El-Samie[1,2] · Heba A. Fayed[3] · Moustafa H. Aly[3]

Received: 13 June 2023 / Accepted: 13 August 2023 / Published online: 7 October 2023

Abstract

Simultaneous measurement of human immunodeficiency virus (HIV) genome DNA hybridization and the DNA melting temperature in a prism-based surface plasmon resonance (SPR) biosensor is modeled theoretically using a simple dual-channel construction. The proposed sensor consists of a BK7 prism coated with silver as a plasmonic material. The metal surface is divided into two channels to detect medium refractive index (RI) and temperature. One half is covered with zinc selenide (ZnSe) semiconductor to enhance the hybridization detection sensitivity and to protect silver from oxidation. The other half is covered with polydimethylsiloxane (PDMS) polymer to detect the temperature variations. The proposed sensor is optimized numerically, and the optimum structure provides an excellent sensitivity of 208 deg/RIU, thanks to the use of the ZnSe layer, which is greater than double the reported dual-channel prism-based sensor in thickness. The polymer channel shows high sensitivity to the temperature variations of − 0.125 deg/°C, which is nearly 10 times the response of the RI channel to temperature variations. The data obtained from the polymer channel is used to compensate for the thermal perturbations of the sensing medium RI, and at the same time, to monitor the increments of the temperature in order to avoid reaching the DNA melting temperature. A mathematical expression is provided to consider the effect of the temperature variations on the RI of the sensing medium to get a better accurate detection process. The DNA hybridization detection of HIV is theoretically discussed in detail starting from the preparation of the sensing medium with the different ingredients until the hybridization between probe and complementary target DNA (ct-DNA) molecules.

Keywords Dual-channel biosensor · Surface plasmon resonance (SPR) · Zinc selenide (ZnSe) · DNA hybridization · DNA melting temperature

Moustafa H. Aly: OSA Member

Extended author information available on the last page of the article

1 Introduction

The SPR biosensors depend on monitoring of the RI variations due to the molecular interaction between pre-immobilized biomolecules on or near a metal–dielectric interface and a liquid sample in real-time form. These biosensors are currently used to measure different parameters, such as sample concentration, kinetics of biomolecular interaction and binding constants (Shpacovitch et al. 2020).

There are many applications that gained a lot from the SPR concept. Most of these applications are vital, as they are concerned with a large number of humans. Diabetes is one of the most spreading diseases around the world, and many researches discussed the possible ways to detect the glucose level in urine instead of blood, as it is a more painless method (Yadav et al. 2021, 2022, 2023; Karki et al. 2022a, b, c; El-assar et al. 2023). Another critical field is the detection of cancerous cells (Karki et al. 2022a, b, c). On the other hand, many researches focused on the improvement of sensor structure, materials and performance to be applicable in different fields (Karki et al. 2022a, b, c; Singh et al. 2023; Karki et al. 2023a, b; Karki et al. 2023a, b).

One of the important fields that SPR bio-sensors are devoted to is the detection of DNA hybridization process. In present days, studying the DNA structure is considered an effective tool for diagnosing many kinds of fatal diseases (Wei et al. 2010), and as a result, the DNA hybridization detection has become more important. The DNA hybridization produces a double-stranded helical structure, whose health and stability are affected by temperature. At a certain temperature, called melting temperature, the DNA structure starts to break. For that reason, it is necessary to monitor temperature to maintain an accurate process.

To this date, researchers developed many SPR biosensor configurations; most of them are dedicated to measure only one parameter. According to the aforementioned literature, dual-channel sensors turn into a must to compensate for the effect of one parameter. Few prism-based configurations are designed to monitor multiple parameters. In (Monzón-Hernández et al. 2018), the authors introduced a simple prism-based SPR sensor for dual-parameter sensing. They proposed simultaneous measurements of RI and temperature, but with a limited sensitivity.

In this paper, a dual-channel prism-based SPR sensor is modelled and theoretically investigated. The proposed sensor is intended to detect the changes of sample RI; namely for DNA hybridization in one channel and temperature in the other channel. This work is the premiere to use a dual-channel prism-based SPR sensor to monitor the DNA hybridization process with emphasis on the effect of temperature on the hybridization quality. All calculations are performed with Matlab.

The rest of this paper is organized as follows. Section 2 illustrates the modeling and design of the proposed sensor. Then, Sect. 3 provides the obtained results and discussions. Section 4 is devoted to the main conclusions.

2 Proposed SPR sensor: model and design

2.1 Theoretical modeling

The proposed SPR sensor configuration is based on Kretschmann model (Kretschmann and Reather 1968). In this model, it is assumed that the prism is covered with a metallic

layer, and a sensing medium is placed over this layer. According to the SPR principle, when a light beam travels through a prism and hits the metallic layer with a certain angle, resonance occurs, resulting in an evanescent wave, which travels laterally along the metal-sensing medium interface with an evanescent field decay length up to hundreds of nanometers (Mazzotta et al. 2014). It can penetrate through the metal layer for a distance of λ/2. As a result, at resonance, there is a decrease in the reflected light intensity, which produces an angle with minimum reflectivity. This angle is called the resonance angle. The target of SPR sensors is to detect this angle and monitor its variations. The resonance angle depends on the RI of the contacting layers, where any change in the RI yields a change in the resonance angle.

The SPR sensors reflectivity is best described by the transfer matrix method (TMM), as it does not contain any approximation that makes it more accurate (Katsidis and Siapkas 2002). To calculate the reflectance or transmittance for a multilayer model, it is assumed that all layers are thin, homogeneous, uniform, isotropic, non-magnetic, and stacked on each other (Yuan et al. 2011).

For a *p*-polarized light, the overall system reflectivity, R_p, can be defined as [7] (Mostufa et al. 2021)

$$R_p = \left| r_p \right|^2 \tag{1}$$

where r_p is the reflection coefficient of the reflected wave, and it is defined for the *N*-layer model as (Mostufa et al. 2021)

$$r_p = \frac{(F_{11} + F_{12}q_N)q_1 - (F_{21} + F_{22}q_N)}{(F_{11} + F_{12}q_N)q_1 + (F_{21} + F_{22}q_N)} \tag{2}$$

Using the matrix of F_{ij} elements, the wave propagation parameters, that describe the light propagation in the *N*-layer model, can be calculated according to the TMM principle as follows (Mostufa et al. 2021; Rahman et al. 2018)

$$F_{ij} = \left[\prod_{k=2}^{N-1} \begin{pmatrix} \cos\beta_k & \frac{-i\sin\beta_k}{q_k} \\ -iq_k \sin\beta_k & \cos\beta_k \end{pmatrix} \right] = \begin{bmatrix} F_{11} & F_{12} \\ F_{21} & F_{22} \end{bmatrix} \tag{3}$$

where β_k and q_k are the random phase constant and the admittance at the kth layer, respectively, and both can be calculated by (Fouad et al. 2017)

$$\beta_k = \frac{2\pi}{\lambda} d_k \sqrt{n_k^2 - (n_p \sin\theta_0)^2} \tag{4}$$

$$q_k = \frac{\sqrt{n_k^2 - (n_p \sin\theta_0)^2}}{n_k^2} \tag{5}$$

where n_k and d_k are the refractive index and thickness of the k^{th} layer, respectively, n_p is the prism refractive index, and θ_0 is the incidence angle at the prism-metal interface.

To ensure the excitation of surface plasmons, the metal and sensing medium dielectric constants must have opposite signs (Barnes et al. 2006). The metal has a large

negative real part of the dielectric constant. To compensate for the ohmic losses that result from electron scattering and absorption of metal, the small imaginary part of the dielectric constant must be considered. On the other side, the sensing medium is considered lossless, which means that it has a positive, real, and small dielectric constant compared to the metal (Tabasi and Falamaki 2018).

To evaluate the system performance, it is mandatory to define its sensitivity which is considered the crucial parameter for any proposed sensor. The sensitivity of a sensor is the resonance angle shift ($\Delta\theta_{SPR}$) due to the change in the sensing medium refractive index (Δn_{sens}), and it can be expressed as (Hossain et al. 2020)

$$S = \frac{\Delta\theta_{SPR}}{\Delta n_{sens}} deg/RIU \tag{6}$$

Another performance parameter is the combined sensitivity factor (CSF), which can be calculated as follows (Cai et al. 2021)

$$CSF = \frac{\partial\theta_{SPR}}{\partial n_s} \times \frac{\left(R_{\max} - R_{\min}\right)}{FWHM} \tag{7}$$

where $\partial\theta_{SPR}$ is the resonance angle shift due to change of the sensing medium RI, ∂n_s, while $R_{\max}$ and $R_{\min}$ are the highest and lowest normalized reflection values of the resonance curve, respectively. The full width at half maximum (FWHM) parameter indicates the quality of the resonance curve, and it should be as small as possible to obtain better sensor sensitivity and detection accuracy (DA).

The figure of merit (*FOM*) of the sensor, or the quality factor (QF) in other words, is an important sensor quantification parameter, which depends on the FWHM of the resonance curve and the sensitivity as follows (Hossain et al. 2020)

$$FOM = \frac{S}{FWHM} RIU^{-1} \tag{8}$$

Better sensor performance requires higher *FOM* values, which can be achieved either by enhancing the near-field intensity to get better spectral shift per refractive index or by reducing the FWHM (also called the resonance linewidth). Reducing the resonance linewidth means reducing the dispersion, which is a challenge as dispersion is a function of the plasmonic losses of the sensor structure (Yang et al. 2023).

The resonance linewidth can be defined as the sum of losses of different sources called damping terms. These losses need to be reduced to get smaller linewidth values. They can be expressed mathematically by (Hartland 2011)

$$\Gamma = \gamma_b + \Gamma_{rad} + \Gamma_{e-surf} + \Gamma_{interface} \tag{9}$$

where γ_b is the bulk damping, which arises from electron scattering in the metal. Γ_{rad} is the radiation damping, which defines the energy loss exhibited during the coupling of plasmonic wave to the radiation field. Γ_{e-surf} is the electron surface scattering damping. $\Gamma_{interface}$ is the interface damping due to losses resulting from the interaction between the metal and the bounded medium over it.

2.2 Field distribution computation through stacked layers

To describe the distribution components of the electric and magnetic fields (E and H) through different layers, the reflectivity and transmittance of the input TM-polarized light is used. The total characteristic matrix is introduced to illustrate the relation between the different components as (Karki et al. 2023a, b)

$$\begin{bmatrix} H_{y1}(z) \\ -E_{x1}(z) \end{bmatrix} = P_1(z).\begin{bmatrix} 1+r_p \\ q_1\left(1-r_p\right) \end{bmatrix} H_y^{inc}, z_1 \le z \le z_2 \tag{10}$$

where r_p and H_y^{inc} are the reflection coefficient and the amplitude of the incident magnetic field, respectively. The propagation matrix $P_1(z)$ is defined as

$$P_1(z) = \begin{bmatrix} \cos\left(\beta_{k(at\,z)}\right) & \frac{i\sin\left(\beta_{k(at\,z)}\right)}{q_1} \\ iq_1\sin\left(\beta_{k(at\,z)}\right) & \cos\left(\beta_{k(at\,z)}\right) \end{bmatrix} \tag{11}$$

For $j \ge 2$,

$$\begin{bmatrix} H_{yj}(z) \\ -E_{xj}(z) \end{bmatrix} = P_j(z)\prod_{j-1}^{1} P\left(z = z_i + d_i\right)\begin{bmatrix} 1+r_p \\ q_1\left(1-r_p\right) \end{bmatrix} H_y^{inc}, z_j \le z \le z_{j+1} \tag{12}$$

where

$$P_j(z) = \begin{bmatrix} \cos\left(\beta_{k(at\,z=z-j)}\right) & \frac{i\sin\left(\beta_{k(at\,z=z-j)}\right)}{q_1} \\ iq_1\sin\left(\beta_{k(at\,z=z-j)}\right) & \cos\left(\beta_{k(at\,z=z-j)}\right) \end{bmatrix} \tag{13}$$

where $H_{yj}(z)$, $E_{xj}(z)$, and $P_j(z)$ are the magnetic fields, electric fields, and propagation matrix, respectively.

The penetration depth of the decaying evanescent wave through the metal surface can be calculated from the imaginary part of the z-component of the wave vector (Tabasi and Falamaki 2018)

$$\delta_d = \frac{1}{K_0}\left[\frac{\varepsilon'_m + \varepsilon_d}{\varepsilon_d^2}\right]^{1/2} \tag{14}$$

where ε'_m and ε_d are the imaginary parts of the metal dielectric constant and the dielectric medium constant, respectively, and K_0 is the wave vector.

The electric field intensity enhancement factor (EFIEF) is a very powerful tool that describes the concentration of the electric field at the proximity of the last layer (sensing layer). The calculation of the EFIEF parameter depends on the electric field and magnetic field components defined as (Karki et al. 2023a, b)

$$\left|\frac{E_{\parallel}\left(\frac{N}{N-1}\right)}{E_{\parallel}\left(\frac{1}{2}\right)}\right|^2 = \frac{\in_1}{\in_n}\left|\frac{H_{y\parallel}\left(\frac{N}{N-1}\right)}{H_{y\parallel}\left(\frac{1}{2}\right)}\right|^2 \tag{15}$$

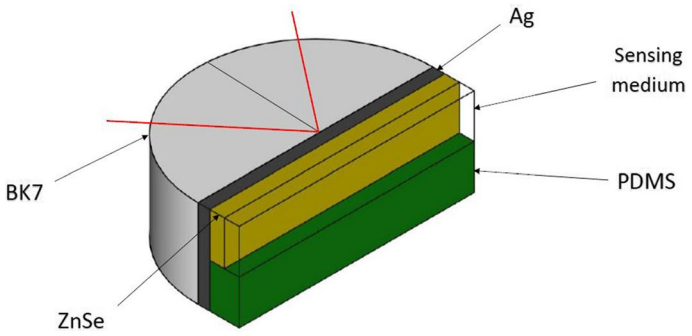

Fig. 1 Proposed sensor structure

2.3 Structure of the proposed sensor

The sensor structure in Fig. 1 is composed of a BK7 coupling prism, a metallic layer of silver (Ag), whose the surface is divided into two sections. One section is used to detect the refractive index change, and it is covered with ZnSe. The other section is covered with a polymer material (PDMS) to detect the temperature variations. The function of the ZnSe layer is to enhance the sensor sensitivity and to protect the silver against oxidation, which may result from the presence of chemicals and different fluids at the sensor surface. ZnSe is a popular semiconductor that is used in the fabrication of many electronic elements, such as solar cells, photodetectors, LEDs, and in-vivo imaging sensors (Zhang et al. 2016). Merging silver and ZnSe materials on one structure was studied deeply in (Chu et al. 2021). The experiments showed an excellent matching between Ag and ZnSe, while studying different parameters, especially the charge transfer (CT). In (El-assar et al. 2023), an excellent sensitivity enhancement was achieved, when using ZnSe over an Ag layer instead of a common gold layer in the SPR biosensor model.

The TM-polarized light is produced by a He–Ne laser source ($\lambda = 633$ nm) to go through the prism and strike its surface. P. Nambisan reported that the use of this wavelength enhances the system sensitivity, as it provides a minimum Kerr effect (Nambisan 2017). Different interrogation techniques were implemented for SPR sensing. They comprise phase interrogation, intensity interrogation, amplitude interrogation, wavelength interrogation, and angle interrogation (Karki et al. 2023a, b). In the proposed sensor, angle interrogation is adopted. K. Brahmachari et al. proved that the type of the prism can affect the sensor performance strongly (Brahmachari and Ray 2013). Their results showed that for a low-refractive-index prism, SPR angle and sensitivity are high with a low dynamic range.

While the main purpose for any biomedical sensor is to provide higher sensitivity, a relatively-low-RI prism, namely BK7, is selected as it has an RI of $n_{BK7} = 1.51508$ (Brahmachari and Ray 2013). Silver is selected as a plasmonic material, because it offers a very sharp resonance dip that means more detection accuracy (Dwivedi et al. 2007). Silver layer covers the prism surface with thickness d_{Ag} and RI $n_{Ag} = 0.06656 + 4.0452i$ (Yuan et al. 2006). ZnSe is placed over a half of the silver layer. It has a thickness d_{ZnSe} and RI $n_{ZnSe} = 2.5780$ (Marple 1964).

The other half of the silver layer is covered with PDMS. This polymer is a very attractive material in the field of temperature sensing, as it offers a higher thermo-optic coefficient (TOC) of -4.66×10^{-4} /°C [19] (Moreno-Hernández et al. 2015) than those of other

polymers. The PDMS has a RI $n_{PDMS} = 1.4118$ (Espinosa-Sánchez et al. 2017). The PDMS is selected to be thick enough with a thickness of 500 nm to isolate it from the sensing medium and make the resonance dip of this channel dependent on the PDMS material only. The sensing medium is placed over the ZnSe channel, and it contains the required test sample with a variable RI n_S.

Although the presented work is a theoretical analysis for the proposed sensor structure, the practical implementation procedure can be taken into account. The proposed sensor can be assembled by the multiple-layer deposition techniques. The first step is to clean the BK7 prism in piranha solution (H_2O_2:$3H_2SO_4$) and several ultrapure water rinses, so that any pollutants are eliminated and then drying is performed with pressurized nitrogen (Akib et al. 2021). The silver layer is to be deposited on the prism surface using an electron-beam evaporation system with a chamber pressure of 1.3×10^{-4} Pa and an evaporation rate of 0.05 nm/s. A real-time monitoring for the deposition rate is achieved with a quartz crystal oscillator (Chen et al. 2010). The PDMS layer is deposited by placing a cuvette on the silver surface at which the PDMS is poured inside to fill half of the total volume. This volume is then cured by heating it up at 60 °C for 4 h (Velázquez-González et al. 2017). The next step is to deposit the ZnSe layer on the other cuvette half using the simple chemical bath deposition method (Lokhande et al. 1998). The deposition of ZnSe depends on the slow release of Zn^{+2} ions from Zn salt with a suitable complexing agent and Se^{-2} ions from selenourea. These ions are condensed on the silver surface in alkaline medium.

3 Results and discussion

As there are two channels with only one laser source, it is assumed that the laser beam strikes the prism surface exactly at the interface between the Ag–ZnSe section and the polymer section. This assumption means that both channels contribute equally to the reflection spectrum, which can be estimated mathematically by (Monzón-Hernández et al. 2018)

$$R_{total} = \frac{1}{2}\left|r_p(sample)\right|^2 + \frac{1}{2}\left|r_p(polymer)\right|^2 \tag{16}$$

Due to the propagation of the laser beam through both channels, there will be two independent resonance dips in the reflectance curve. The first dip (θ_S) represents the resonance due to the metal-ZnSe channel, which is controlled by the variation of n_S. The other dip (θ_P) is produced due to the polymer channel, and its movement depends on n_{PDMS}.

The proposed biosensor is designed to detect the DNA hybridization process with real-time temperature monitoring to avoid reaching the DNA melting temperature. To get the best performance, each layer thickness is studied independently.

The metal layer thickness is studied, while using a 1-nm ZnSe layer, assuming that the sensing layer contains phosphate-buffered saline (PBS) without any DNA ($n_S = 1.335$) at 25 ℃, Fig. 2a, and then containing (BSA + Strep. + dsDNA) ($n_S = 1.34$) at 25 ℃ (Kukanskis et al. 1999), Fig. 2b. It is clear, from Fig. 2, that changing the silver layer thickness affects the resonance angle for both channels. The polymer channel is thick enough to be isolated from the sensing medium RI change. For that, only the SPR angle for the sensing medium is considered. From Fig. 2, an increase is observed in the SPR angle, when the sensing medium RI increases from 1.335 to 1.34 ($\Delta n_S = 0.005$). When $d_{Ag} = 30$ nm, the SPR curve is distorted; when $d_{Ag} = 40$ nm, the SPR angle increases from 69.7 deg to 70.3 deg ($\Delta\theta_{SPR} = 0.6\ deg$); when $d_{Ag} = 50$ nm, the SPR angle moves from 69.7 deg

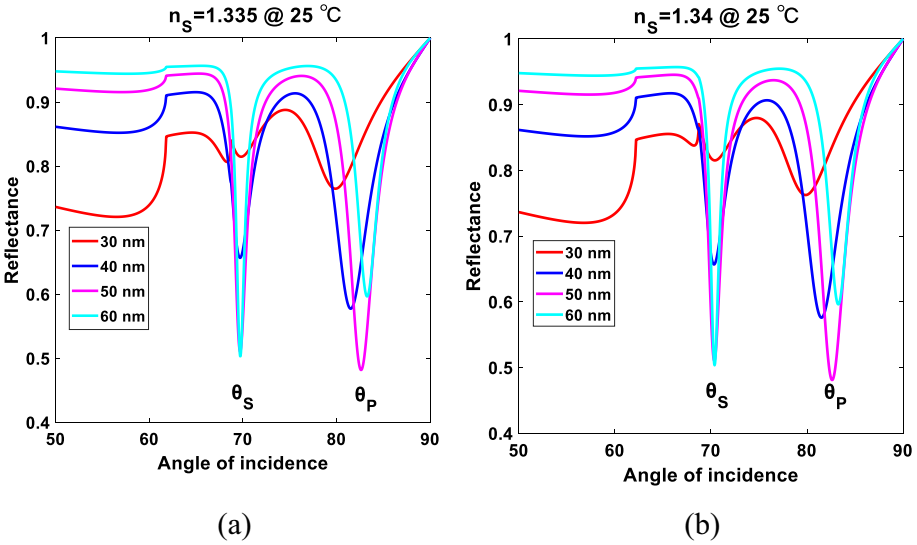

Fig. 2 Proposed sensor performance at different Ag thicknesses **a** for the sensing medium containing only PBS without DNA, **b** for the BSA + Strep. + dsDNA scenario

Table 1 Sensitivity (S) for different Ag layer thicknesses

d_{Ag}(nm)	$n_S = 1.335$ θ_{SPR} (deg)	$n_S = 1.34$ θ_{SPR} (deg)	$\Delta\theta_{SPR}$(deg)	S (deg/RIU)
30	–	–	–	–
40	69.7	70.3	0.6	120
50	69.7	70.34	0.64	128
60	69.74	70.38	0.64	128

to 70.34 deg ($\Delta\theta_{SPR} = 0.64\ deg$); and when $d_{Ag} = 60$ nm, the SPR angle increases from 69.74 deg to 70.38 deg ($\Delta\theta_{SPR} = 0.64\ deg$). The obtained results are summarized in Table 1. The results show that at 50 and 60 nm, the SPR angle shift is the same, but at 50 nm, the reflectance curve is the best with a perfect dip at both channels for both cases, which makes it the best thickness.

To study the effect of the ZnSe layer thickness on the proposed sensor sensitivity, it is assumed that the Ag layer thickness is 50 nm and the sensing layer one time is bare (no DNA and $n_S = 1.335$) and the other time is containing BSA + Strep. + dsDNA ($n_S = 1.34$) at 25 ℃. Figure 3a shows an almost similar response for those of the sensors with different ZnSe layer thicknesses when the sensing medium is bare. In contrary, when BSA + Strep. + dsDNA molecules are added, Fig. 3b, the curves and sensitivity are widely affected. When the sensing medium RI is increased from 1.335 to 1.34 ($\Delta n_S = 0.005$), the SPR angles increase. From Fig. 3, when $d_{ZnSe} = 5$ nm, the SPR angle increases from 73.58 to 74.42 deg ($\Delta\theta_{SPR} = 0.84\ deg$); when $d_{ZnSe} = 6$ nm, the SPR angle is shifted from 74.94 deg to 75.83 deg ($\Delta\theta_{SPR} = 0.89\ deg$); and when $d_{ZnSe} = 7$ nm, the SPR angle increases from 76.47 deg to 77.51 deg ($\Delta\theta_{SPR} = 1.04\ deg$); but at $d_{ZnSe} = 8$ nm, the SPR angle is shifted from 78.39 deg to 79.79 deg ($\Delta\theta_{SPR} = 1.4\ deg$) and the reflectance curve is distorted when BSA + Strep. + dsDNA molecules are added. Table 2 summarizes all

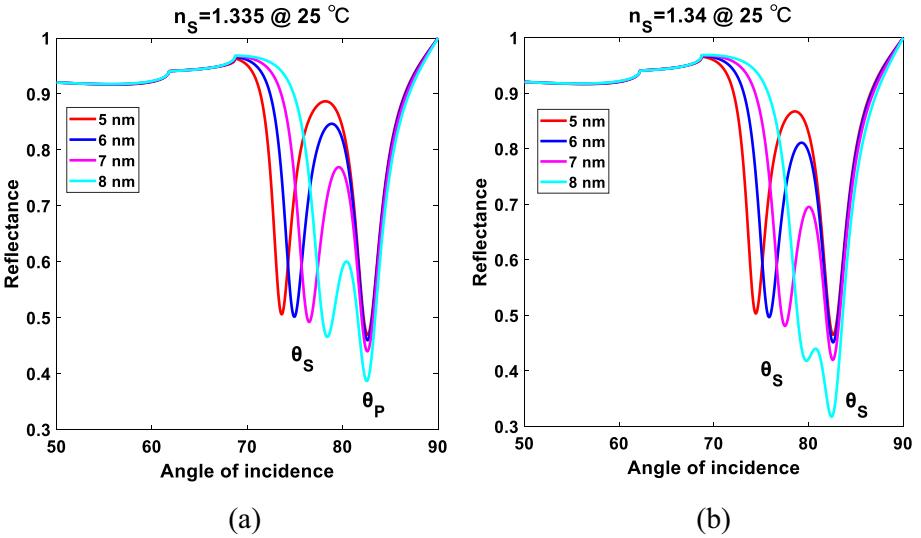

Fig. 3 Proposed sensor performance at different ZnSe thicknesses **a** when the sensing medium contains only PBS without DNA, **b** when BSA + Strep. + dsDNA are present

Table 2 Sensitivity (S) for different ZnSe layer thicknesses

d_{ZnSe}(nm)	$n_S = 1.335\theta_{SPR}$ (deg)	$n_S = 1.34\theta_{SPR}$ (deg)	$\Delta\theta_{SPR}$(deg)	S (deg/RIU)
5	73.58	74.42	0.84	168
6	74.94	75.83	0.89	178
7	76.47	77.51	1.04	208
8	78.39	79.79	1.4	280

obtained results. The calculated sensitivities are 168, 178, 208, and 280 deg/RIU at 5, 6, 7 and 8 nm, respectively. The sensitivity for the polymer channel is 0 deg/RIU for all thicknesses. Although the 8-nm thickness provides the best sensitivity, the curve shape, which contributes to the resulting accuracy, is not the best. For that, a 7-nm thickness is selected, as it provides the optimum sensitivity and curve shape.

The effect of temperature variations on the medium RI and polymer is investigated. This effect is negligible for prism and metal, when using angle interrogation method, and it is presented strongly in the wavelength interrogation method (Kai-Qun et al. 2007). Consequently, this effect is not considered on both components. The reflectance curve is studied, assuming that $d_{Ag} = 50$ nm, $d_{ZnSe} = 7$ nm and the sensing medium is water ($n_S = 1.333$). Changing the temperature from 20 ℃ to 50 ℃ results in a change in the sample and polymer refractive indices, which translates into a negative shift (left shift) for the SPR angle of both channels as shown in Fig. 4. The amount of shift for θ_P is larger than that for θ_S as PDMS has a TOC of -4.66×10^{-4} /°C, and water has a TOC of -0.8×10^{-4} /°C (Kamikawachi et al. 2008). From Fig. 4, the sensitivity levels of the PDMS channel and water channel are -0.125 deg/°C and -0.012 deg/°C, respectively.

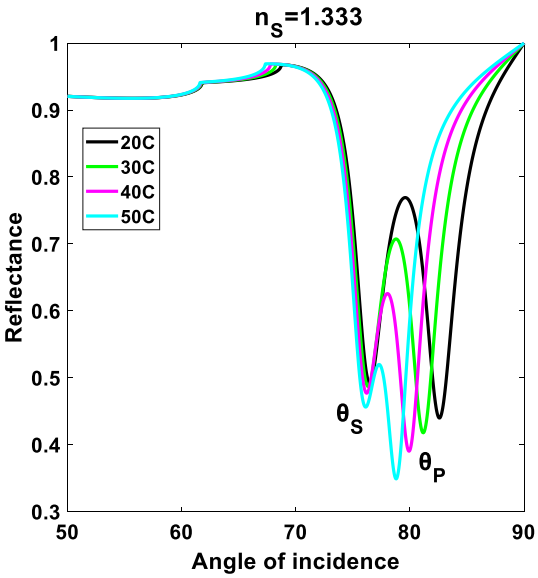

Fig. 4 Proposed sensor performance at different temperatures

The resonance angle shift for the PDMS channel is 10.4 times the shift of the water channel, which proves the high sensitivity of the polymer for the temperature variations.

To that end, one can conclude that, the change in the resonance angle for the sensing medium depends on the change in the medium RI, and at the same time, on the temperature even if the temperature change is very small. The change in the medium RI due to the temperature should be compensated for to get more accurate results. For the purpose of monitoring of the DNA melting temperature, we notice an increase in medium temperature by observing the change in θ_P.

The obtained RI and temperature sensitivity results due to the shift of resonance angles for both channels, θ_S and θ_P, are recorded. When the sensing medium RI changes, the sensitivity is 208 and 0 deg/RIU for the sensing medium and polymer channels, respectively. When the temperature is varied, the sensitivity becomes -0.012 and -0.125 deg/°C for the sensing medium and polymer channels, respectively. These results can be summarized in the following matrix

$$\begin{bmatrix} \theta_S \\ \theta_P \end{bmatrix} = \begin{bmatrix} -0.012 & 208 \\ -0.125 & 0 \end{bmatrix} \begin{bmatrix} \Delta T \\ \Delta n \end{bmatrix} \tag{17}$$

which can be rearranged as

$$\begin{bmatrix} \Delta T \\ \Delta n \end{bmatrix} = \frac{1}{26} \begin{bmatrix} 0 & -208 \\ 0.125 & -0.012 \end{bmatrix} \begin{bmatrix} \theta_S \\ \theta_P \end{bmatrix} \tag{18}$$

where θ_S and θ_P are in degrees, the temperature change (ΔT) is in degrees Celsius, and the RI change (Δn) is in RIU.

Table 3 Comparison between the sensitivity levels of the proposed sensor and other biosensors

Configuration	Sensitivity (deg/RIU)	References
Single-channel Au-MoS_2-graphene-based biosensor	89.29	Rahman et al. (2017a, b)
Single-channel Ag-graphene-based biosensor	91.76	Maharana et al. (2013)
Single-channel Au-black phosphorus-graphene-based biosensor	125.00	Pal et al. (2018)
Single-channel Au-MoS_2-graphene -based biosensor	130.00	Hossain et al. (2020)
Single-channel Au-WSe_2-graphene-based biosensor	178.87	Nurrohman and Chiu (2020)
Dual-channel Au-based biosensor	98.67	Monzón-Hernández et al. (2018)
Dual-channel Ag-ZnSe-based biosensor	208.00	Presented work

By solving Eq. (9), one can get the amount of the RI change as a function of the sensing medium resonance angle and the temperature change as follows

$$\Delta n = 4.8 \times 10^{-3}\theta_S + 5.75 \times 10^{-5}\Delta T \tag{19}$$

From Eq. (10), one can compensate for the impact of temperature variations on the sensing medium RI using the second term, hence improving the accuracy of the whole DNA hybridization detection process.

Table 3 provides a comparison between the obtained sensitivity for the proposed sensor and different models in the literature.

4 DNA hybridization detection

The DNA hybridization can be either a complementary or non-complementary. The complementary DNA hybridization, Fig. 5a, is achieved when two single-stranded DNA (ssDNA) molecules are combined to produce a double-stranded DNA (dsDNA), one is a probe molecule (p-DNA) and the other is a target that has a matched nucleotide sequence. When both molecules are mismatched, no hybridization occurs, and this is called non-complementary DNA hybridization as shown in Fig. 5b. (Haque and Rouf 2021).

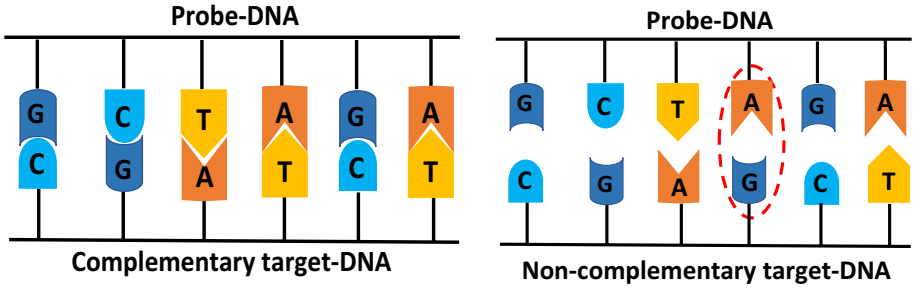

Fig. 5 DNA hybridization process results **a** complementary target-DNA, **b** non-complementary target-DNA

The DNA hybridization process produces a change in the sensing medium molar concentration, which changes the medium refractive index. The change in the medium refractive index leads to a clear movement of the SPR angle, which can be measured with the proposed sensor. The variation of the medium refractive index due to adsorption of the DNA molecules can be calculated as follows (Shushama et al. 2017; Rahman et al. 2017a, b; Diéauez et al. 2009)

$$n_s^1 = n_s^0 + C_a \frac{\Delta n}{\Delta C} \tag{20}$$

where n_s^1 and n_s^0 are the sensing medium refractive indices after and before adsorption of DNA molecules, respectively, C_a is the concentration of the adsorbed DNA molecules, and $\Delta n/\Delta C$ is the increment in the sensing medium refractive index after adding the DNA molecules.

The thermodynamic properties of DNA molecules, such as melting temperature (T_m), can be used to predict the nature of hybridization, computationally. The DNA melting temperature, also called DNA denaturation temperature, is the temperature at which half of the probe and target DNA molecules are hybridized successfully in double-helical structures, and the other half remain unhybridized. T_m provides useful information about the duplex stability (Alvarado-González et al. 2009). To guarantee perfect DNA hybridization detection, T_m should be monitored through the whole process.

In this section, the DNA hybridization detection approach for HIV genome is theoretically illustrated depending on the experimental data presented in (Kukanskis et al. 1999) with simultaneous detection of temperature in the other channel. The proposed sensor is composed of a BK7 prism with 50 nm of Ag covering its surface. Above silver, there are two channels; one is coated with a 7-nm ZnSe layer and it is devoted for hybridization detection, and the other is coated with 500 nm of PDMS polymer to detect the temperature variations. The sensing layer is assumed to contain phosphate-buffered saline (PBS), which is modified by biotinylated bovine serum albumin (b-BSA) and

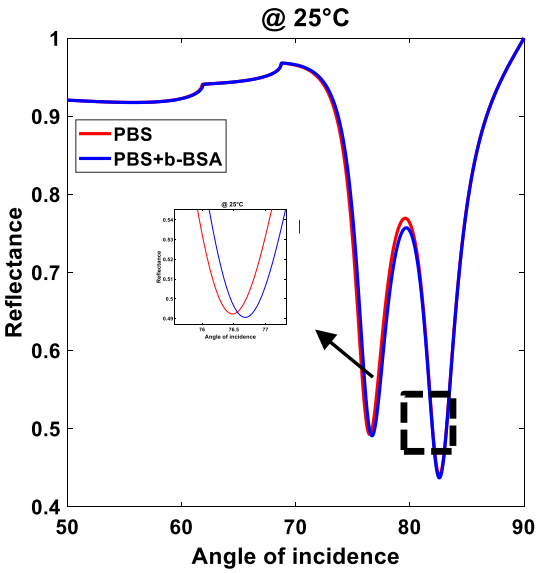

Fig. 6 Reflectance of the proposed sensor, when the sensing medium contains PBS and after adding b-BSA.

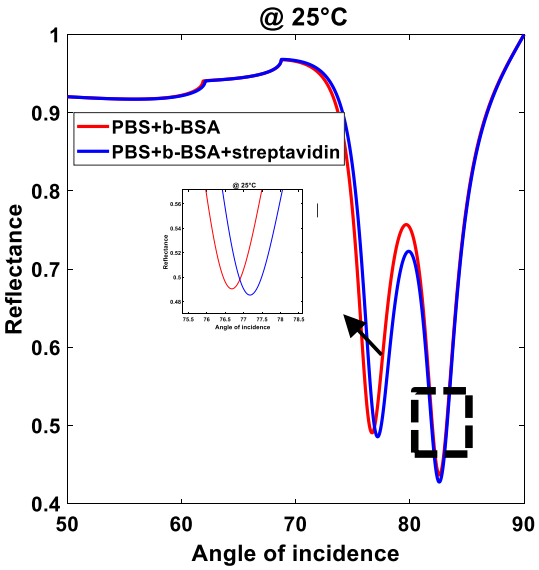

Fig. 7 Reflectance of the proposed sensor after streptavidin is added to PBS with b-BSA

streptavidin proteins to perfectly capture and anchor the probe DNA molecules, biotinylated oligonucleotides, to the ZnSe surface. The resonance angle shift is numerically calculated after adding each of the ingredients.

Figure 6 shows the resonance angle shift if b-BSA is added to the PBS solution. It is clear that the resonance angle moves from 76.47 deg for PBS to 76.67 deg after adding 0.67 mg/ml of b-BSA with a sensitivity of 200 deg/RIU, while the polymer channel remains constant.

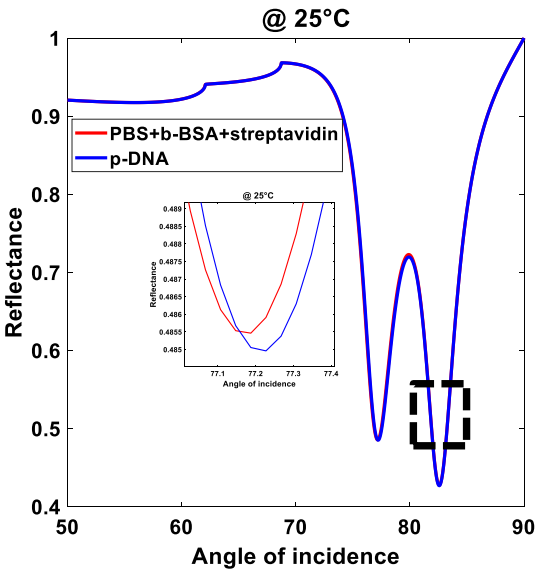

Fig. 8 Reflectance of the proposed sensor after immobilizing probe DNA in the PBS with b-BSA and streptavidin

Figure 7 illustrates how the resonance angle of the mixture is affected after adding streptavidin. It is noticeable that the resonance angle is shifted from 76.67 deg for b-BSA in PBS to 77.19 deg after adding 0.33 mg/ml of streptavidin, and the temperature channel remains without change. The proposed sensor detects the presence of the streptavidin with a sensitivity of 216.66 deg/RIU.

The change of the medium RI after adding the probe DNA, 3 µg/µl biotinylated deoxyribonucleotide probes, to the b-BSA and streptavidin in the PBS solution will lead to a change in the resonance angle as clarified in Fig. 8. The SPR angle is shifted from 77.19 to 77.23 deg with a sensitivity of 200 deg/RIU and 0 deg/RIU for temperature channel.

Two different samples of complementary target-DNA can be used to detect the HIV genome hybridization with the pre-immobilized probes. The first sample is composed of 3 µg/µl of Acomp and Bcomp sequences. The obtained results for the hybridization process are presented in Fig. 9. The reflectance curves in Fig. 9 show a shift of the SPR angle after adding the target DNA sequences from 77.23 to 77.35 deg with a sensitivity of 200 deg/RIU.

The second complementary target sample is 0.8 µg/µl of 291-base-long HIV PCR product. The reflectance and SPR angle shift for the hybridization process of the probe and target samples are displayed in Fig. 10. The addition of the PCR product to the probe leads to a change in the sensing medium RI due the hybridization process. The change in the medium RI drives the SPR angle to shift from 77.23 to 77.43 deg with a sensitivity of 200 deg/RIU.

5 Conclusion

In this paper, we presented a premier dual-channel prism-based SPR biosensor model for HIV-DNA hybridization detection with DNA melting temperature monitoring. The proposed biosensor model structure is optimized to get very high sensitivity values. The sensor reaches a sensitivity of 208 deg/RIU for the RI channel and 0 deg/RIU for the temperature

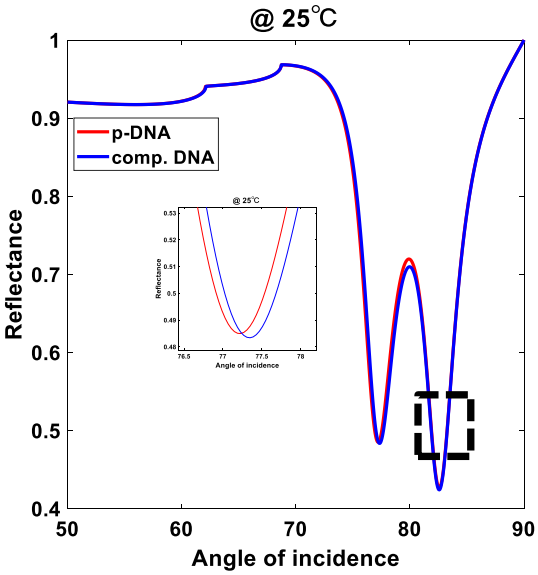

Fig. 9 Reflectance of the proposed sensor, when the sensing medium contains probe DNA, and after adding ct-DNA

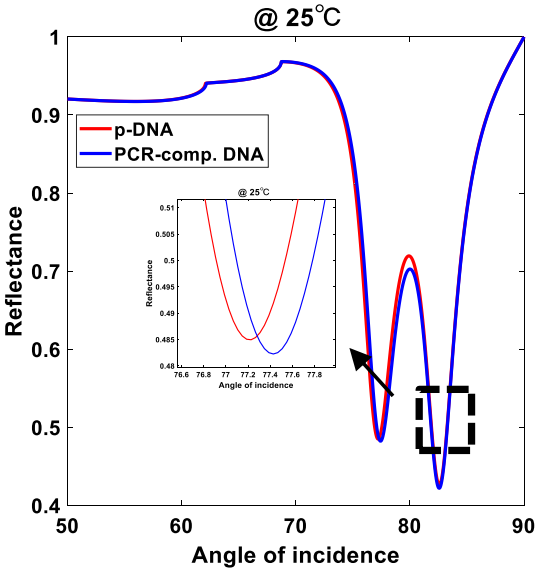

Fig. 10 Reflectance of the proposed sensor, when the sensing medium contains probe DNA, and after adding PCR amplified ct-DNA product

channel at constant temperatures. The effect of temperature on the sensing medium and PDMS channel is studied. The obtained results showed a shift of the resonance angles for both channels, when temperature is increased and the sensitivities are −0.012 and −0.125 deg/°C for the sensing medium and polymer channels, respectively. A temperature channel data is used to compensate for the thermal perturbations in the sensing medium RI and at the same time to monitor the increment of the temperature to avoid reaching the DNA melting temperature. A mathematical expression is provided to consider the effect of the temperature variations on the RI value of the sensing medium to get more accurate detection process. The feasibility of the proposed model to detect DNA hybridization for HIV genome is discussed in detail. The proposed sensor can detect the hybridization process with a very high sensitivity of 200 deg/RIU.

Author Contributions All authors have directly participated in the planning, execution, and analysis of this study. They have read and approved the final version of the manuscript.

Funding Open access funding provided by The Science, Technology & Innovation Funding Authority (STDF) in cooperation with The Egyptian Knowledge Bank (EKB). The authors did not receive any funds to support this research.

Data availability The data used and/or analyzed during the current study are available from the corresponding author on reasonable request.

Declarations

Competing interests The authors declare that they have no competing interests.

References

Akib, T.B.A., Mou, S.F., Rahman, M.M., Rana, M.M., Islam, M.R., Mehedi, I.M., Mahmud, M.A.P., Kouzani, A.Z.: Design and numerical analysis of a graphene-coated SPR biosensor for rapid detection of the novel coronavirus. Sensors **21**(10), 3491 (2021)

Alvarado-González, M., Crozier, P.S., Flores, N., Gallo, M., Orrantia-Borunda, E., Glossman-Mitnik, D.: Computational prediction of the melting temperature of a DNA biosensor to detect mycobacterium tuberculosis. J. Mol. Struct. (thoechem) **912**, 60–62 (2009)

Barnes, W.L.: Surface plasmon-polariton length scales: a route to sub-wavelength optics. J. Opt. a: Pure Appl. Opt. **8**(4), S87–S93 (2006)

Brahmachari, K., Ray, M.: Effect of prism material on design of surface plasmon resonance sensor by admittance loci method. Front. Optoelectron. **6**(2), 185–193 (2013)

Cai, H., Shan, S., Wang, X.: High sensitivity surface plasmon resonance sensor based on periodic multilayer thin films. Nanomaterials (basel) **11**(12), 3399 (2021)

Chen, W., Thoreson, M.D., Ishii, S., Kildishev, A.V., Shalaev, V.M.: Ultra-thin ultra-smooth and low-loss silver films on a germanium wetting layer. Opt. Express **18**(5), 5124–5134 (2010)

Chu, Q., Han, B., Jin, Y., Guo, S., Jin, S., Park, E., Chen, L., Jung, Y.M.: Surface plasmon resonance induced charge transfer effect on the Ag-ZnSe-PATP system. Spectrochim. Acta Part A Mol. Biomol. Spectrosc. **248**, 119167 (2021)

Diéauez, L., Darwish, N., Mir, M., Martínez, E., Moreno, M., Samitier, J.: Effect of the refractive index of buffer solutions in evanescent optical biosensors. Sens. Lett. **7**(5), 851–855 (2009)

Dwivedi, Y.S., Sharma, A.K., Gupta, B.D.: Influence of skew rays on the sensitivity and signal-to-noise ratio of a fiber-optic surface plasmon-resonance sensor: a theoretical study. Appl. Opt. **46**, 4563–4569 (2007)

El-assar, M., Taha, T.E., El-Samie, F.E.A., Fayed, H.A., Aly, M.H.: ZnSe-based highly-sensitive SPR biosensor for detection of different cancer cells and urine glucose levels. Opt. Quant. Electron. **55**, 76 (2023)

Espinosa-Sánchez, Y.M., Luna-Moreno, D., Rodríguez-Delgado, M., Sánchez-Álvarez, A.: Determination of optical parameters of organic and inorganic thin films using both surface plasmon resonance and Abelès-Brewster methods. Optik **142**, 426–435 (2017)

Fouad, S., Sabri, N., Poopalan, P., Jamal, Z.A.Z.: Surface plasmon resonance sensor sensitivity enhancement using gold-dielectric material. Int J Nanoelectron Mater **10**, 147–156 (2017)

Haque, T., Rouf, HK.: DNA hybridization detection using graphene-MoSe2–Ag heterostructure-based surface plasmon resonance biosensor. Appl. Phys. A **127**, 759 (2021)

Hartland, G.V.: Optical studies of dynamics in noble metal nanostructures. Chem. Rev. **111**, 3858–3887 (2011)

Hossain, B., Kabir, A., Hossain, S.H., Islam, K.H.Z., Hossain, S., Pathan, M.I., Mondol, N., Abdulrazak, L.F., Hossain, A., Rana, M.: Numerical modeling of MoS2–graphene bilayer-based high-performance surface plasmon resonance sensor: structure optimization for DNA hybridization. Optical Engineering **59**(10), 105105 (2020)

Kai-Qun, L., Lai-Ming, W., Dou-Guo, Z., Rong-Sheng, Z., Pei, W., Yong-Hua, L., Hai, M.: Temperature effects on prism-based surface plasmon resonance sensor. Chin. Phys. Lett. **24**(11), 3081–3084 (2007)

Kamikawachi, R.C., Abe, I., Paterno, A.S., Kalinowski, H.J., Muller, M., Pinto, J.L., Fabris, J.L.: Determination of thermo-optic coefficient in liquids with fiber Bragg grating reflectometer. Opt. Commun. **281**(4), 621–625 (2008)

Karki, B., Jha, A., Pal, A., Srivastava, V.: Sensitivity enhancement of refractive index-based surface plasmon resonance sensor for glucose detection. Opt. Quant. Electron. **54**, 595 (2022a)

Karki, B., Ramya, K.C., Sandhya Devi, R.S., Srivastava, V., Pal, A.: Titanium dioxide, black phosphorus and bimetallic layer-based surface plasmon biosensor for formalin detection: numerical analysis. Opt. Quant. Electron. **54**, 451 (2022b)

Karki, B., Uniyal, A., Pal, A., Srivastava, V.: Advances in surface plasmon resonance-based biosensor technologies for cancer cell detection. Int J Opt **2022**, 1476254 (2022c)

Karki, B., Ansari, G., Uniyal, A., Srivastava, V.: $PtSe_2$ and black phosphorus employed for sensitivity improvement in the surface plasmon resonance sensor. J Comput Electron **22**, 106–115 (2023a)

Karki, B., Uniyal, A., Srivastava, V., Pal, A.: Black phosphorous and cytop nanofilm-based long-range spr sensor with enhanced quality factor. J Sens **2023**, 2102915 (2023b)

Katsidis, Ch.C., Siapkas, D.I.: General transfer-matrix method for optical multilayer systems with coherent, partially coherent, and incoherent interference. Appl. Opt. **41**(19), 3978–3987 (2002)

Kretschmann, E., Reather, H.: Radiative decay of non-radiative surface plasmons excited by light. Zeit. Natur. **23**(12), 2135–2136 (1968)

Kukanskis, K., Elkind, J., Melendez, J., Murphy, T., Miller, G., Garner, H.: Detection of DNA hybridization using the TISPR-1 surface plasmon resonance biosensor. Anal. Biochem. **274**, 7–17 (1999)

Lokhande, C.D., Patil, P.S., Tributsch, H., Ennaoui, A.: ZnSe thin films by chemical bath deposition method. Sol. Energy Mater. Sol. Cells **55**(4), 379–393 (1998)

Maharana, P.K., Padhy, P., Jha, R.: On the field enhancement and performance of an ultra-stable SPR biosensor based on graphene. IEEE Photonics Technol. Lett. **25**(22), 2156–2159 (2013)

Marple, D.T.F.: Refractive index of ZnSe, ZnTe, and CdTe. J. Appl. Phys. **35**, 539–542 (1964)

Mazzotta, F., Johnson, T.W., Dahlin, A., Shaver, J., Oh, S., Hook, F.: Influence of the evanescent field decay length on the sensitivity of plasmonic nanodisks and nanoholes. ACS Photonics **2015**(2), 256–262 (2014)

Monzón-Hernández, D., Velázquez-González, J.S., Luna-Moreno, D., Torres-Cisneros, M., Hernández-Roma, I.: Prism-based surface plasmon resonance for dual-parameter sensing. IEEE Sensors **18**(10), 4030–4037 (2018)

Moreno-Hernández, C., Monzón-Hernández, D., Hernández-Romano, I., Villatoro, J.: Single tapered fiber tip for simultaneous measurements of thickness refractive index and distance to a sample. Opt. Exp. **23**(17), 22141–22148 (2015)

Mostufa, S., Paul, A.K., Chakrabarti, K.: Detection of hemoglobin in blood and urine glucose level samples using a graphene-coated SPR based biosensor. OSA Continuum **4**(8), 2164–2176 (2021)

Nambisan, P.: An Introduction to Ethical Safety and Intellectual Property Rights Issues in Biotechnology. Elsevier, Newyork (2017)

Nurrohman, D.T., Chiu, N.F.: Surface plasmon resonance biosensor performance analysis on 2D material based on graphene and transition metal dichalcogenides. ECS J. Solid State Sci. Technol. **9**, 115023 (2020)

Pal, S., Verma, A., Raikwar, S., Prajapati, Y.K., Saini, J.P.: Detection of DNA hybridization using graphene-coated black phosphorus surface plasmon resonance sensor. Appl. Phys. A **124**(394), 1–11 (2018)

Rahman, M.S., Anower, M.S., Hasan, M.R., Hossain, M.B., Haque, M.I.: Design and numerical analysis of highly sensitive Au– Mos2-graphene-based hybrid surface plasmon resonance biosensor. Opt. Commun. **396**, 36–43 (2017a)

Rahman, M.S., Anower, M.S., Rahman, Md.K., Hasan, Md.R., Hossain, Md.B., Haque, Md.I.: Modeling of highly sensitive MoS2-graphene hybrid based fiber optic SPR biosensor for sensing DNA hybridization. Optik **140**, 989–997 (2017b)

Rahman, M.S., Rikta, K.A., Bin Bashar, L., Anower, M.: Numerical analysis of graphene coated surface plasmon resonance biosensors for biomedical applications. Optik **156**, 384–390 (2018)

Shpacovitch, V., Hergenroder, R.: Surface plasmon resonance (SPR)-based biosensors as instruments with high versatility and sensitivity. Sensors **20**(11), 3010 (2020)

Shushama, K.N., Rana, Md.M., Inum, R., Hossain, Md.B.: Graphene coated fiber optic surface plasmon resonance biosensor for the DNA hybridization detection: simulation analysis. Opt. Commun. **383**, 186–190 (2017)

Singh, T.I., Singh, P., Karki, B.: Early detection of chikungunya virus utilizing the surface plasmon resonance comprising a silver-silicon-$PtSe_2$ multilayer Structure. Plasmonics **18**, 1173–1180 (2023)

Tabasi, O., Falamaki, C.: Recent advancements in the methodologies applied for the sensitivity enhancement of surface plasmon resonance sensors. Anal. Methods **10**(32), 3906–3925 (2018)

Velázquez-González, J.S., Monzón-Hernández, D., Martínez-Piñón, F., May-Arrioja, D.A., Hernández-Romano, I.: Surface plasmon resonance-based optical fiber embedded in PDMS for temperature sensing. IEEE J. Sel. Top. Quantum Electron. **23**(2), 126–131 (2017)

Wei, F., Lillehoj, P.B., Ho, C.M.: DNA diagnostics: nanotechnology-enhanced electrochemical detection of nucleic acids. Pediatr. Res. **67**(5), 458–468 (2010)

Yadav, A., Sudhanva, S., Sharan, P., Kumar, A.: Modeling, simulation and computational analysis of plasmonic optical sensor using $BaTiO_3$ in diabetes mellitus. Int. J. Inf. Technol. **13**, 2163–2168 (2021)

Yadav, A., Kumar, A., Sharan, P.: Sensitivity enhancement of a plasmonic biosensor for urine glucose detection by employing black phosphorous. J. Opt. Soc. Am. B **39**, 200–206 (2022)

Yadav, A., Kumar, A., Sharan, P., Mishra, M.: Highly sensitive bimetallic-metal nitride SPR biosensor for urine glucose detection. IEEE Trans. Nanobiosci. (2023). https://doi.org/10.1109/TNB.2023.3246535
Yang, K., Chen, Y., Yan, S., Yang, W.: Nanostructured surface plasmon resonance sensors: toward narrow linewidths. Heliyon **9**(6), e16598 (2023)
Yuan, X.C., Ong, B.H., Tan, Y.G., Zhang, D.W., Irawan, R., Tjin, S.C.: Sensitivity-stability-optimized surface plasmon resonance sensing with double metal layers. J. Opt. A Pure Appl. Opt. **8**(11), 959–963 (2006)
Yuan, Y., Ding, L., Guo, Z.: Numerical investigation for SPR-based optical fiber sensor. Sens Actuators B **157**(1), 240–245 (2011)
Zhang, Q., Li, H., Ma, Y., Zhai, T.: ZnSe nanostructures: synthesis, properties and applications. Prog. Mater Sci. **83**, 472–535 (2016)

Authors and Affiliations

Mohamed El-assar[1] · Taha E. Taha[1] · Fathi E. Abd El-Samie[1,2] · Heba A. Fayed[3] · Moustafa H. Aly[3]

✉ Moustafa H. Aly
mosaly@aast.edu

Mohamed El-assar
mr_assar46@yahoo.com

Taha E. Taha
taha117@hotmail.com

Fathi E. Abd El-Samie
fathi_sayed@yahoo.com

Heba A. Fayed
hebam@aast.edu

[1] Faculty of Electronic Engineering, Electronics and Electrical Communications Engineering Department, Menoufia University, Menouf, Egypt

[2] Department of Information Technology, College of Computer and Information Sciences, Princess Nourah Bint Abdulrahman University, P.O. Box 84428, Riyadh 11671, Saudi Arabia

[3] Electronics and Communications Engineering Department, College of Engineering and Technology, Arab Academy for Science, Technology and Maritime Transport, Alexandria, Egypt